Design of a high energy density experiment to measure the suppression of hydrodynamic instability in an applied magnetic field

Zoe Barbeau,[1] Kumar Raman,[2] Mario Manuel,[3] Sabrina Nagel,[2] and Bhimsen Shivamoggi[4]
[1)]*Stanford University, Stanford, CA 94305, USA*
[2)]*Lawrence Livermore National Laboratory, Livermore, CA 94550 USA*
[3)]*General Atomics, San Diego, CA 92121, USA*
[4)]*University of Central Florida, Orlando, FL 32816*

(*Electronic mail: zbarbeau@stanford.edu)

(Dated: 5 November 2021)

A transverse magnetic field can suppress the hydrodynamic instability growth of an unstable plasma interface. This effect, of interest to inertial confinement fusion and astrophysics, has mostly been studied via simulation. Here we present the design of an experiment at the National Ignition Facility (NIF) to demonstrate this effect in a laboratory. Simulations indicate the time scale for the diffusion of the magnetic field across the mixing region should be at least comparable to the time scale of the instability growth in order to have a measurable suppression effect. This motivates the use of lower density target materials than usual high energy density (HED) hydrodynamics experiments to permit faster hydrodynamics and higher plasma conductivities (through higher temperature), for a given laser drive and magnetic field. We discuss a target design for creating a Rayleigh–Taylor unstable HED plasma interface that uses 320 mg/cc iodine-doped carbon foam as the heavy material, 20 mg/cc carbon foam as the light material, and a 6 μm amplitude, 120 μm wavelength ripple machined at the interface, that shows a measurable suppression effect with a nominal NIF drive and a 30 T magnetic field (the present facility limit). Models indicate lower density foams may display even larger suppression effects, as the hohlraum drive also radiatively preheats the foam to permit even higher temperatures, hence higher conductivities. (LLNL-JRNL-825494-DRAFT)

I. INTRODUCTION

A transverse magnetic field suppresses the growth of a hydrodynamically unstable interface.[1] This effect could explain the smooth interface morphology of the Crab Nebula, as the strong magnetic field would tend to suppress fine scale instability growth that would otherwise occur along the filaments of swept up supernova ejecta.[2,3] This effect is also relevant for magnetized inertial confinement fusion (ICF).[4–6] However, studies of this effect have been mostly numerical,[7–12] and experimental attempts to see it have been (so far) inconclusive.[13] Here we assess the possibility of demonstrating this effect at the National Ignition Facility (NIF).[14]

We start with a platform based on Ref. 15 (Figure 1a), which is a typical geometry for studying hydrodynamic instabilities in the high energy density (HED) regime.[16] The NIF laser creates a ∼230 eV x–ray bath in the gold halfraum, sending a blast wave into a planar target package consisting of iodinated carbon plastic (CHI, 1.43 g/cc) and carbon resorcinol foam (CRF, 0.1 g/cc) with a sinusoidal perturbation (6 μm amplitude, 120 μm wavelength) machined at the interface. The blast wave converts the solid target into an impulsively–accelerated plasma interface with the imprinted initial condition. The interface develops by action of the Richtmyer–Meshkov (RMI) and Rayleigh–Taylor (RTI) instabilities, with late–time secondary structure induced by the Kelvin–Helmholtz instability (KHI) (Figure 1b).[17]

Figure 1a depicts a 30 T magnetic field coil attached to the Ref. 15 package. This is presently the highest field allowed on NIF, based on assessments of the probability of optical damage due to shrapnel from the exploding target,[18] to which the massive coil is a dominant contribution. While somewhat larger magnetic fields may eventually be possible,[19,20] the

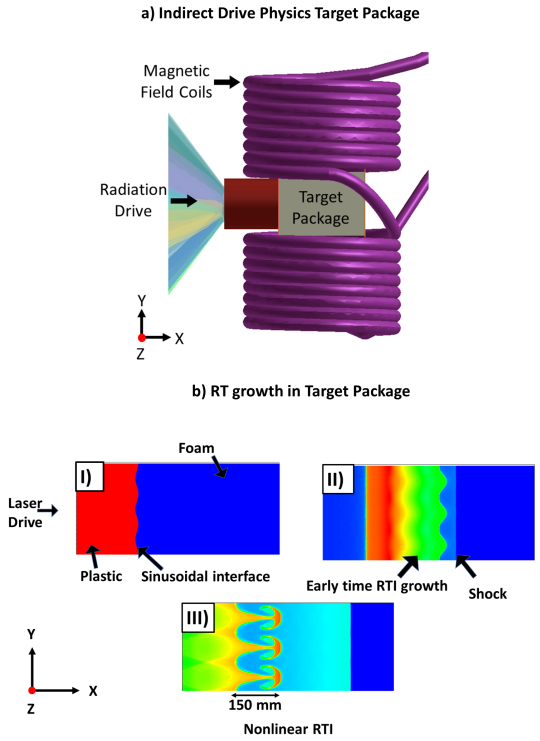

FIG. 1. a) shows the target package, radiation drive from NIF, and magnetic coils. b) shows the RTI growth where I) is CHI plastic as the heavy material and carbon resorcinol foam, II) is early time RTI growth, and III) is nonlinear RTI

magnetic field cannot be made arbitrarily large. This makes the finite conductivity of the plasma a key design issue.

To understand the importance of conductivity, we first consider the linear regime RTI growth rate of a uniformly accelerated, incompressible, magnetized plasma interface assuming *infinite* conductivity, i.e. ideal magnetohydrodynamics (MHD):[1]

$$\eta_B^2 = gkA_T - \frac{B^2k^2\cos^2\theta}{2\pi(\rho_1+\rho_2)} \quad (1)$$

Here g is the acceleration, $k \equiv \frac{2\pi}{\lambda}$ the wavenumber, B the magnetic field, θ the angle between $\vec{B}$ and $\vec{k}$, ρ_1 and ρ_2 the densities of the light and heavy fluids respectively, and $A_T \equiv \frac{\rho_1-\rho_2}{\rho_1+\rho_2}$ the Atwood number.

Eq. 1 indicates the component of the magnetic field along the interface suppresses RTI at short wavelengths in a manner similar to surface tension.[21] While the NIF experiment is in a more complex regime involving non-uniform acceleration, multiple instabilities (RTI, RMI, and KHI), compressible fluids, and a perturbation amplitude of order the wavelength, ideal MHD simulations are nonetheless consistent with Eq. 1. The simulations indicate a strong suppression effect with a 30 T initial B_y field (Figures 2) that starts in the linear regime and persists as the interface grows (Figure 3). While Eq. 1 implies that a B_x field alone will not cause suppression, the simulation indicates 2D MHD flows near the interface will generate a small B_y component from an initial B_x field. While this induced B_y field has a small effect on the growth of the seeded wavelength (Figure 3), it does suppress instability growth at smaller length scales, such as the KHI features (Figure 2).

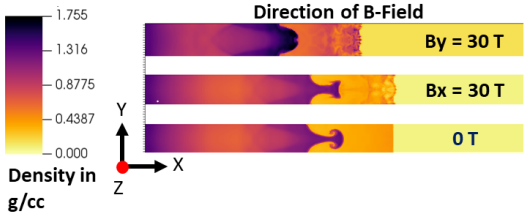

FIG. 2. Suppression of RTI under 30 T B-Field in Different Directions in Ideal MHD with 1.43 g/cc CHI plastic as the heavy pusher material and 80 mg/cc CRF as the foam

Modeling the effect of finite conductivity requires a resistive MHD simulation with a conductivity model. The Spitzer model[22] is, perhaps, the simplest to implement:

$$\sigma = \frac{3(4\pi\varepsilon_0)^2(T)^{\frac{3}{2}}}{4\sqrt{2\pi}Z_*^2 m^{\frac{1}{2}}\ln\Lambda} \quad (2)$$

Here ε_0 is the permittivity of free space, k_B is Boltzmann's constant, T the temperature in eV, Z_* the ionization state, m the electron mass, and $\ln\Lambda$ the Coulomb logarithm. If we repeat the simulations assuming Spitzer conductivity, the suppression effect disappears entirely (Figure 4). This is consistent with theoretical work[23] showing that an otherwise RT

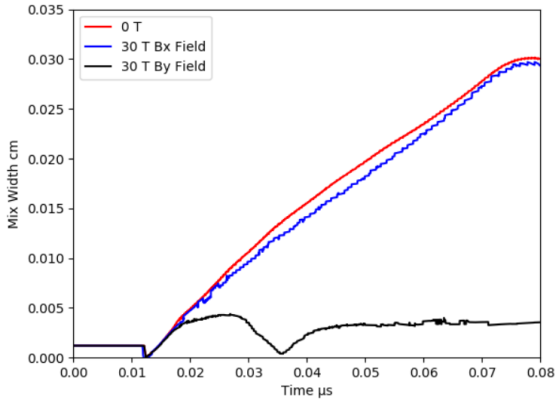

FIG. 3. Mix width vs. time shows the significant suppression of RTI under 30 T By-Field in Ideal MHD with 1.43 g/cc CHI plastic as the heavy pusher and 80 mg/cc CRF as the foam

stable mode can become overstable and grow exponentially in the presence of finite resistivity effects (the growth rate scaling as $\sim \sigma^{-1/3}$).

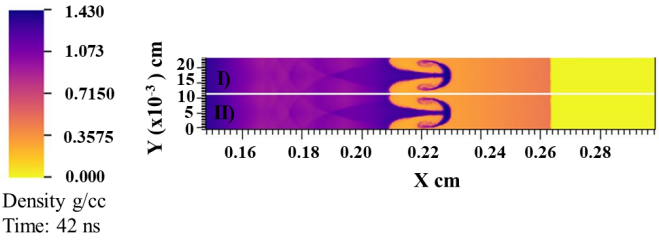

FIG. 4. Effect of 30 T magnetic field on nominal target package in resistive MHD using Spitzer Conductivity: no RTI suppression is observed for a 30 T By-field in I) compared to a 0 T By-field in II)

In ideal MHD, the magnetic flux tubes are frozen into the fluid. The flux tubes are compressed by the shock, which amplifies the magnetic field, then twisted by vortical motions induced by instability, which generates magnetic tension that opposes the instability. This is also generates a B_y field from an initial B_x field and vice versa. In contrast, in resistive MHD, the magnetic field can diffuse ahead of the shock and away from the interface before magnetic tension builds up. While there is some evidence that the Spitzer model might underestimate the plasma conductivity in HED regimes,[24–26] the typical HED hydrodynamic instability experiment appears to be in a resistive MHD regime.[13] Therefore, the key design issue for an HED experiment aiming to see the suppression effect is to speed up the hydrodynamics relative to the magnetic diffusion, to allow build up of the magnetic tension that drives the effect.

This leads us towards lower density materials than are used in typical HED hydrodynamic instability experiments. For a given drive, lower density materials will have faster hydrodynamics and slower magnetic diffusion, the latter due to higher conductivities resulting from higher temperatures (c.f. Eq. 2). Similarly, it is advantageous to optimize the laser pulse to

achieve high target temperatures, usually by maximizing the energy. After discussing our modeling setup and these ideas more explicitly, we present a low density point design (320 mg/cc CHI, 20 mg/cc CRF) for which models predict a measurable suppression effect in a 30 T B_y field. We also discuss even lower density designs that show a larger suppression effect but introduce new complications. We conclude with the implications of our study for a NIF experiment.

II. MODEL SETUP

The simulations in this paper use ARES,[27] a radiation hydrodynamics code with a resistive MHD package developed at Lawrence Livermore National Laboratory. The model includes single group radiation diffusion, tabulated equations of state and opacities, and a Thomas–Fermi type model for ionization. We perform three types of MHD simulations: (1) Ideal MHD calculations, (2) Resistive MHD calculations that assign a constant conductivity to all materials, and (3) Resistive MHD calculations that use a Spitzer model to calculate the conductivity in each zone. We expect (3) to be the most accurate model while (1) and (2) are convenient for physics studies.

The simulations are driven by a radiation temperature boundary condition based on a hohlraum calculation of the NIF laser pulse, discussed in Ref. 15. The simulations in this paper scale the Ref. 15 temperature source by a 1.15× multiplier, corresponding to about 1.75× higher laser energy (i.e. $E \sim T_r^4$ where E is the energy and T the radiation temperature). Laser energies of this order have been demonstrated in this platform.[28] The scaled source is a step towards optimizing the drive for high target temperatures.

III. PHYSICS DESIGN PRINCIPLES

The magnetic force per unit volume in cgs units is:

$$\frac{1}{c}\vec{J}\times\vec{B} = \frac{1}{4\pi}(\vec{B}\cdot\nabla)\vec{B} - \nabla\frac{B^2}{8\pi} \tag{3}$$

Here J is the current density, c is the speed of light, and we ignore the displacement current. The two terms on the RHS are called the magnetic tension force and magnetic pressure force respectively. The magnetic tension term can be further decomposed:

$$\frac{1}{4\pi}(B\cdot\bigtriangledown)B = \frac{B^2}{8\pi}\frac{\hat{n}}{R_c} + \hat{b}\hat{b}\cdot\bigtriangledown\frac{B^2}{8\pi} + \tag{4}$$

where $\hat{b}$ is the unit vector in the direction of the local magnetic fluid, $\hat{n}$ is the normal pointing towards the center of curvature of the local magnetic field, and R_c is the radius of curvature. The first term is directed towards the center of curvature of the magnetic field lines, and provides a restoring force to straighten bent magnetic field lines.[7] The second term cancels with the magnetic pressure in Eq. 3, so that only components of the magnetic pressure gradient perpendicular to the local field exert force on the plasma. Because of this second term, the magnetic tension and magnetic pressure terms of Eq. 3 are not independent. As we will show, the magnetic tension force is about twice as large in magnitude as the magnetic pressure force at experiment conditions, but both effects contribute towards the instability suppression.

Finite conductivity weakens these forces by diffusing the magnetic gradients that generate them. We can infer the scaling from the magnetic diffusion equation:

$$\frac{\partial\vec{B}}{\partial t} = \frac{c^2}{4\pi\sigma}\nabla^2\vec{B} \tag{5}$$

where we assume Ohm's Law, $\vec{J} = \sigma\vec{E}$, and again ignore the displacement current. The expression suggests the distance L the magnetic field diffuses in a given time t should scale as $L \sim \sqrt{t/\sigma}$. We can compare this diffusion length with the spatial extent of the mixing region, or "mix width". If L is small compared to the mix width, the system should behave like ideal MHD where the magnetic field does not diffuse. Conversely, if L is much larger than the mixing width, the instability growth would proceed as if the magnetic forces were not present.

Figures 5, 6, and 7 show the role of finite conductivity in the experiment by comparing the Spitzer model simulation in Fig. 4, which calculates a conductivity of about 3 cm/mΩ for both materials over much of the experiment, with constant conductivity calculations with values of 10 cm/mΩ and 100 cm/mΩ respectively.

Figure 5 shows visible instability suppression in the 100 cm/mΩ conductivity case compared to the Spitzer case, both in the mix width and in the vicinity of the KH rollup. The magnetic field jumps by a factor of three across the shock front and remains high in the vicinity of the interface. In the 10 cm/mΩ conductivity case, there is slightly less growth in the KHI rollup off its mushroom cap than the Spitzer calculation. We also see the magnetic field starting to diffuse across the shock front. The Spitzer calculation is nearly identical to zero field, and the magnetic field has diffused away from both the shock and interface.

Figure 6 shows that mix width for the 100 cm/mΩ case deviating early in time from the Spitzer run, while the 10 cm/mΩ deviates later in time and only slightly. This is consistent with the suppression in the 100 cm/mΩ case being both suppression of the linear regime growth of the seeded mode (c.f. Eq. 1) and suppression of the higher modes induced by KHI in the nonlinear regime, while the suppression in the 10 cm/mΩ case is primarily of the higher modes that appear in the nonlinear regime. We note that, similar to RTI, an otherwise KH stable mode can become overstable and grow exponentially in the presence of finite resistivity effects.[29]

Fig 7 plots the magnetic forces and fluid vorticity for the three conductivity cases. In general, regions of high magnetic force correlate with locations of high fluid vorticity, consistent with a picture where twisting fluid motions also twist the magnetic flux, generating tension. The magnetic tension is about twice as large as the magnetic pressure. The 100 cm/mΩ conductivity run has lower vorticity at the interface than the lower

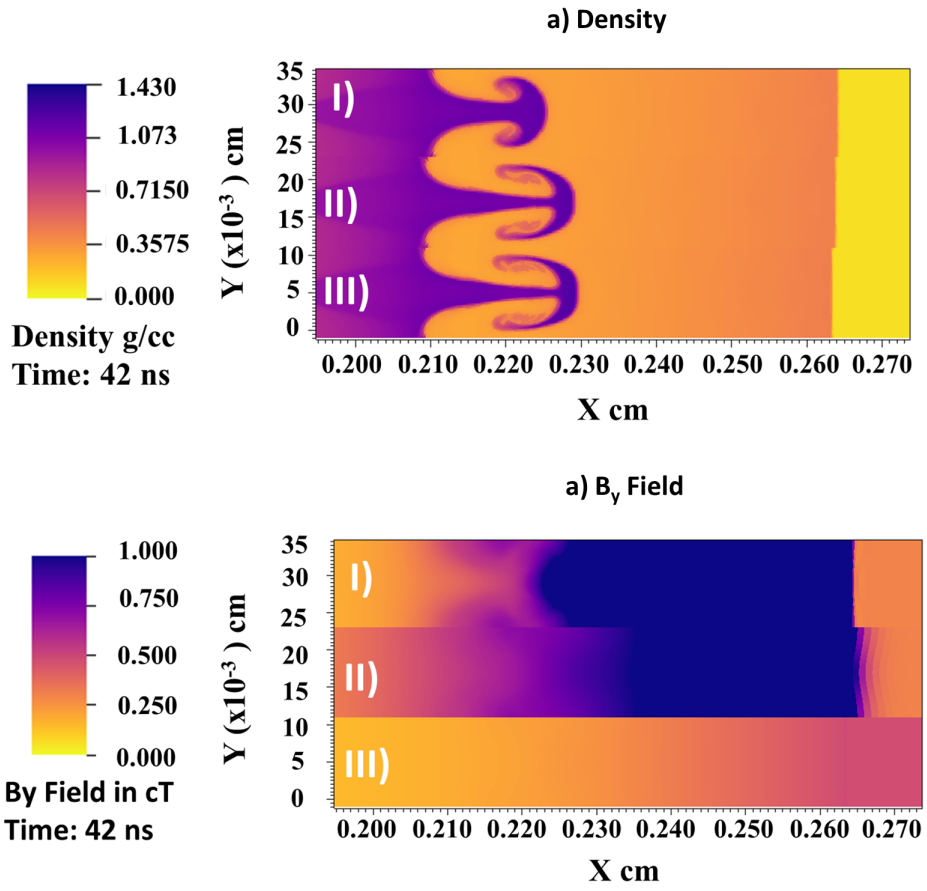

FIG. 5. Effect of 30 T B-field on I) 100 cm/mΩ constant conductivity model, II) 10 cm/mΩ constant conductivity model, III) Spitzer conductivity model

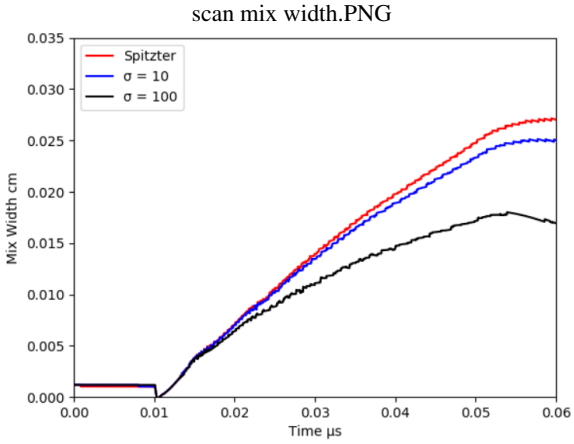

FIG. 6. Mix width as a function of time is shown for 100 cm/mΩ constant conductivity model, 10 cm/mΩ constant conductivity model, and Spitzer conductivity model under a 30 T B-field

conductivity runs because the magnetic restoring forces are much higher.

In practice, minimizing L means designing the interface to grow quickly (minimizing t) while having as high a conductivity as possible. Both aspects are helped by moving to lower density materials.

IV. LOW DENSITY TARGET PACKAGE

Figures 8 shows Spitzer model calculations with and without a 30 T B_y field for a low density point design using 320 mg/cc CHI as the heavy material,[30] 20 mg/cc carbon foam as the light material, and a 6 μm amplitude, 120 μm wavelength initial perturbation. The drive is the same as the high density target. The simulation predicts a visible suppression of both the mix width and of the KHI rollups.

The target hydrodynamics is qualitatively similar to the high density design, but the interface moves faster (Figure 9 ab). The model predicts higher plasma temperature (50 eV vs. 10 eV) and conductivity (15 cm/mΩ vs. 3 cm/mΩ) for the low density design, which is sufficient to keep the magnetic field from diffusing ahead of the shock and to remain high in the vicinity of the interface (Figure 10 ab). Both designs are

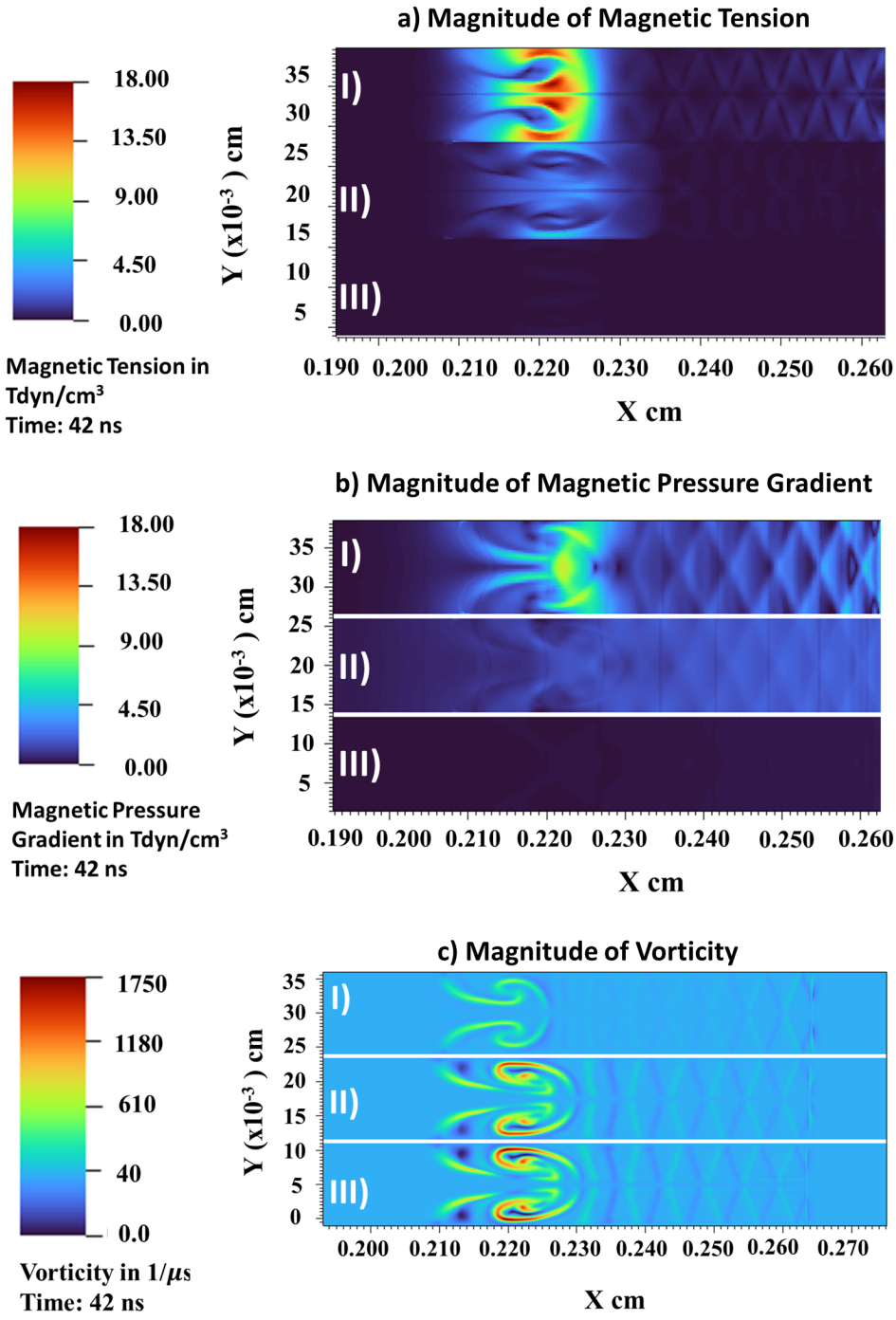

FIG. 7. Effect of 30 T B-field on I) 100 cm/mΩ constant conductivity model, II) 10 cm/mΩ constant conductivity model, III) Spitzer conductivity model. Magnetic tension and magnetic pressure gradients contribute to the suppression of the RTI which can be seen in the reduction in vorticity as these forces increase.

in regimes of high plasma β (defined as the ratio of plasma pressure to magnetic pressure), which is $O(100)$ for the low density design and $O(1000)$ for the high density design, as shown explicitly in Figure 11.

The simulated peak–to–valley mix width (Figure 12) shows the suppression effect starting fairly early in experiment time, though after the perturbation has grown nonlinear. In this particular design, which simply applied the original drive to the new package, a second shock — arising from the reflection of the initial rarefaction off the ablation front (as can be seen in Figure 9b) — recompresses the interface around 12 ns, causing a slight drop in the mix width. While the details may

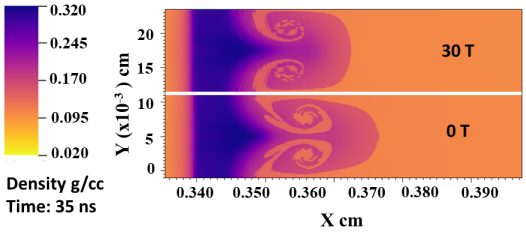

FIG. 8. We see the suppression of the Rayleigh Taylor Instability for a low-density target under a 30 T B_y field

be sensitive to model assumptions, we expect a purely hydrodynamic edge effect like this to be independent of magnetic field, so should not affect a comparison of instability growth with and without a magnetic field.

Simulations predict more instability suppression at even lower densities — as shown in Figure 13 for an 80 mg/cc CHI, 10 mg/cc CRF design — but such designs present new challenges. Very low density targets tend to be difficult to manufacture. Figure 14 compares synthetic radiographs of the (320 mg/cc CHI, 20 mg/cc CRF) and (80 mg/cc CHI, 10 mg/cc CRF) designs showing the low contrast of the latter, mainly due to the very small density difference between "heavy" and "light" materials (c.f. Figure 13). Simulations indicate the larger instability suppression of the very low density design is due, in part, from the hohlraum radiatively preheating the target prior to the main shock, which does not occur for the other designs (Figure 9c). While these issues are not insurmountable, they do complicate the experiment, so we focus our assessment on the (320 mg/cc CHI, 20 mg/cc CRF) design.

The form of the perturbation is another design variable. In the linear regime (amplitude much smaller than the wavelength), the width of the mixing region at a given time is proportional to the initial amplitude, so larger initial amplitudes would help achieve a mixing region comparable to the magnetic diffusion length at that time. However, it is difficult to study this phenomenon directly in the linear regime given the sizes and growth rates involved and the ~ 25 μm spatial resolution of present diagnostics (see Ref. 15 for further discussion). Wavelengths that grow quickly enough to reach a diagnosable size within the experiment duration tend to be nonlinear by that point. Figure 15 compares the (6 μm amplitude, 120 μm wavelength) design with ripples having twice (12 μm) and half (3 μm) the initial amplitude. The 6 μm case shows a clearer difference, with and without a B_y field, than the 3 μm case. However, nonlinear saturation[31] appears to eliminate any obvious advantage to using larger initial amplitudes than this. Similarly, we find no obvious advantage to varying the wavelength to twice or half as large: longer wavelengths grow too slowly while shorter wavelengths saturate more quickly.

Finally, Figure 16 scans the magnetic field. Marginally increasing the B_y magnetic field from 30 T to 40 T lessens the Kelvin–Helmholtz roll-ups, while a 60 T B_y-field completely suppresses the roll-ups and appreciably reduces the spike length. The 30 T field appears to be close to the minimum field necessary to see this suppression effect with the (320 mg/cc CHI, 20 mg/cc CRF) design. Therefore, even marginal improvements to the NIF current coils could be significant for this experiment.

Lower density designs seem to provide additional margin for seeing the suppression effect. Advances in target fabrication and imaging techniques (e.g., higher spatial resolution[32] or phase contrast imaging[33]) could improve the viability of such designs. Moreover, we can consider intentionally preheating the materials.[34] A full assessment would require higher fidelity models of the hohlraum drive and radiation flow through the target.

We expect a hohlraum x–ray drive to be comparatively insensitive to an imposed 30T magnetic field, based on simulations of plasma conditions near the hohlraum wall and recent data, making indirect–drive a convenient approach for direct comparisons with and without a field.[35] We can also consider direct–drive, if we account for (or verify as negligible) the effect of the magnetic field on transport properties like electron conduction that could lead to differences in how the laser couples to the target, with and without a magnetic field.[36] However, all in all, our study suggests it is feasible to demonstrate the phenomenon of hydrodynamic instability suppression by a magnetic field experimentally at NIF.

V. SUMMARY

HED experiments studying magnetized hydrodynamic instabilities must consider resistive effects. In order to see the suppression of RTI by a magnetic field, the length scale for the diffusion of the magnetic field must be comparable to, and ideally less than, the width of the mixing region. Low density target materials are a way to achieve this. An hohlraum–driven design with a (320 mg/cc CHI, 20 mg/cc CRF) target package shows a small but measurable suppression effect, with similar but faster hydrodynamic behavior as standard, denser targets. Lower density designs appear to show even greater suppression effects, assisted by more complex physics, particularly radiative preheat from the hohlraum.

VI. DATA AVAILABILITY

The data that supports the findings of this study are available within the article.

ACKNOWLEDGMENTS

We thank Lee Ellison, Will Farmer, and Dave Strozzi for helpful discussions on MHD modeling. This work was performed under the auspices of the U.S. Department of Energy by Lawrence Livermore National Laboratory under Contract DE-AC52-07NA27344.

This document was prepared as an account of work sponsored by an agency of the United States government. Neither

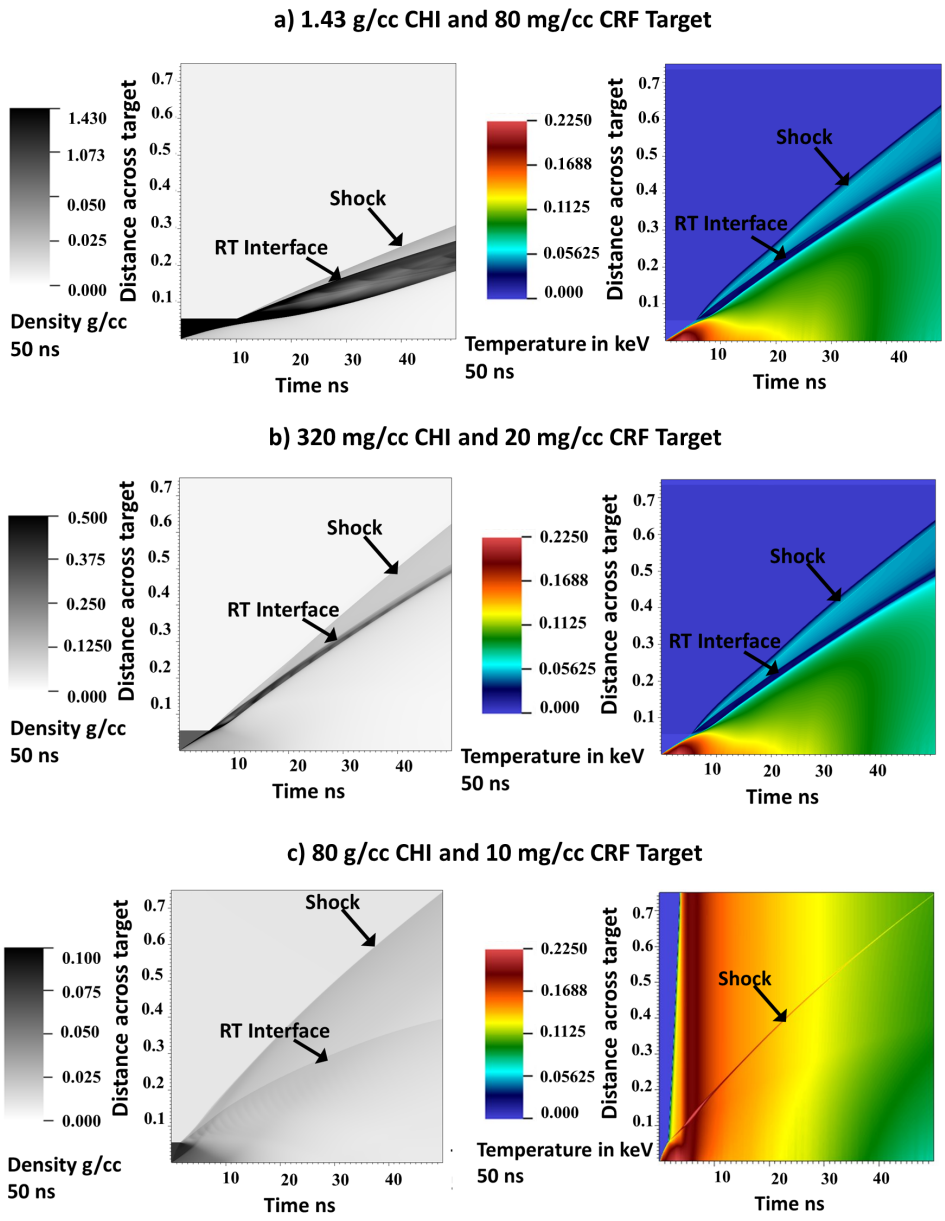

FIG. 9. The time history plots show a centerline slice of the target at each time. c) shows the preheating effect in the low density targets where the target is heated ahead of the shock. The nominal target a) and 320 mg/cc CHI and 20 mg/cc CRF target do not have preheating.

[1]B. K. Shivamoggi, Zeitschrift fr angewandte Mathematik und Physik ZAMP **33**, 693 (1982).
[2]J. J. Hester, J. M. Stone, P. A. Scowen, B.-I. Jun, I. Gallagher, John S., M. L. Norman, G. E. Ballester, C. J. Burrows, S. Casertano, J. T. Clarke, D. Crisp, R. E. Griffiths, J. G. Hoessel, J. A. Holtzman, J. Krist, J. R. Mould, R. Sankrit, K. R. Stapelfeldt, J. T. Trauger, A. Watson, and J. A. Westphal, Astrophysical Journal **456**, 225 (1996).
[3]J. J. Hester, Annu. Rev. Astron. Astrophys **46**, 127 (2008).
[4]S. A. Slutz and R. A. Vesey, Phys. Rev. Lett. **108**, 025003 (2012).
[5]L. J. Perkins, B. G. Logan, G. B. Zimmerman, and C. J. Werner, Physics of Plasmas **20**, 072708 (2013).
[6]B. Srinivasan and X. Tang, Physics of Plasmas **20**, 056307 (2013).

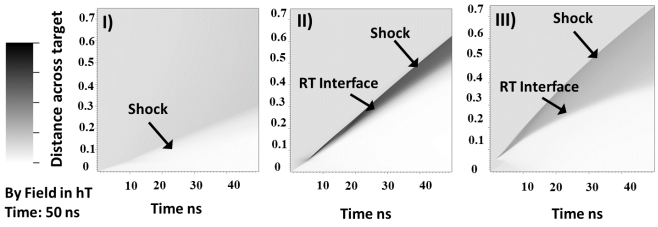

FIG. 10. The time history plots of the magnetic fields of I) 1.43 g/cc CHI, 80 mg/cc CRF target, II) 320 mg/cc CHI, 20 mg/cc CRF target, and III) 80 mg/cc CHI, 10 mg/cc CRF target shows the magnetic field diffusing across the target for the 1.43 g/cc CHI, 80 mg/cc CRF target. However, it is seen that the magnetic field no longer diffuses across the target and is amplified by the shock for the 320 mg/cc CHI, 20 mg/cc CRF target and 80 mg/cc CHI, 10 mg/cc CRF target.

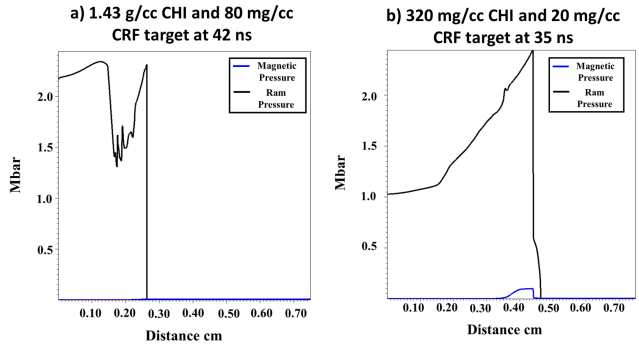

FIG. 11. Ram pressure and magnetic pressure across the centerline of the target at 42 ns and 35 ns respectively.

chi crf 20 PTV curves.PNG

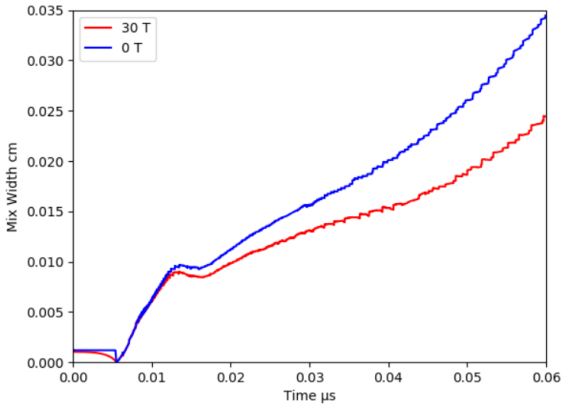

FIG. 12. The mix width plotted versus time shows the suppression of the Rayleigh Taylor Instability for a low-density target under a 30 T B_y field

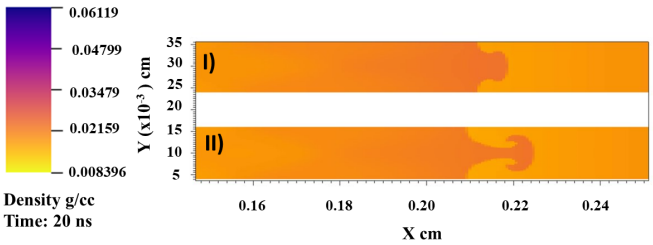

FIG. 13. Significant suppression is observed for a 80 mg/cc CHI, 10 mg/cc CRF target where I) has a 30 T B_y-Field and II) has a 0 T B_y-Field

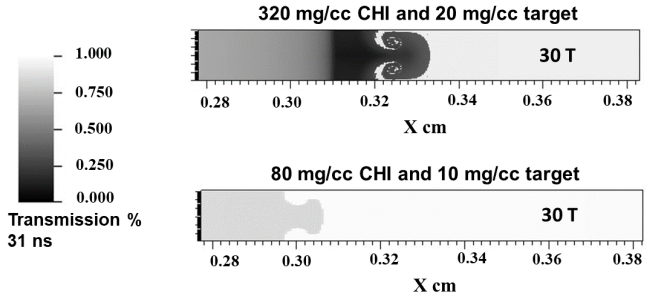

FIG. 14. A mock radiograph showing the opacity of the RT growth is sufficient to be observed experimentally compared for the 320 mg/cc CHI, 20 mg/cc CRF target compared to the 80 mg/cc CHI, 10 mg/cc CRF target. The radiographs assume a 9 keV backlighter.

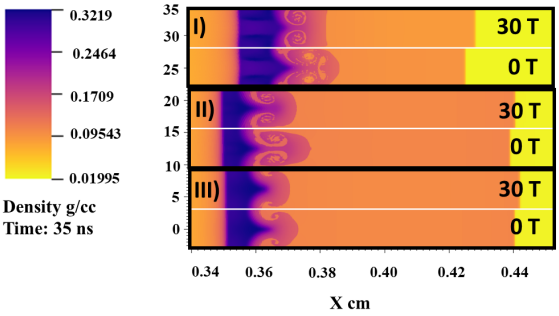

FIG. 15. 320 mg/cc CHI and 20 mg/cc CRF target with 120 μm wavelength and I) 12 μm amplitude II) 6 um amplitude III) 3 μm amplitude

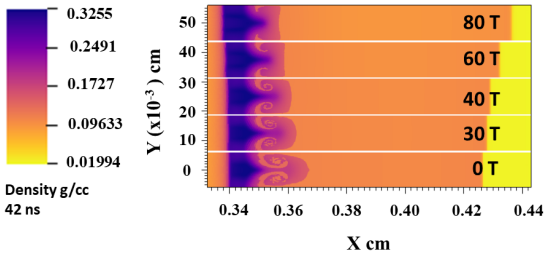

FIG. 16. Effect of By-field strength on 320 mg/cc CHI and 20 mg/cc CRF target

[7] B. I. Jun, M. L. Norman, and J. M. Stone, Astrophysical Journal **453**, 332 (1995).
[8] J. M. Stone and T. Gardiner, Physics of Fluids **19**, 094104 (2007).
[9] J. M. Stone and T. Gardiner, The Astrophysical Journal **671**, 1726 (2007).
[10] S. Liberatore and S. Bouquet, Phys. Fluids **20**, 116101 (2008).
[11] O. Porth, S. S. Komissarov, and R. Keppens, MNRAS **443**, 547 (2014).

[12]J. Carlyle and A. Hillier, Astronomy and Astrophysics **605**, A101 (2017).
[13]M. J.-E. Manuel, B. Khiar, G. Rigon, B. Albertazzi, S. R. Klein, F. Kroll, F. E. Brack, T. Michel, P. Mabey, S. Pikuz, J. C. Williams, M. Koenig, A. Casner, and C. C. Kuranz, Matter and Radiation at Extremes **6**, 026904 (2021).
[14]E. I. Moses, R. N. Boyd, B. A. Remington, C. J. Keane, and R. Al-Ayat, Physics of Plasmas (1994-present) **16**, 041006 (2009).
[15]S. R. Nagel, K. S. Raman, C. M. Huntington, S. A. MacLaren, P. Wang, M. A. Barrios, T. Baumann, J. D. Bender, L. R. Benedetti, D. M. Doane, S. Felker, P. Fitzsimmons, K. A. Flippo, J. P. Holder, D. N. Kaczala, T. S. Perry, R. M. Seugling, L. Savage, and Y. Zhou, Physics of Plasmas **24**, 072704 (2017).
[16]B. A. Remington, H.-S. Park, D. T. Casey, R. M. Cavallo, D. S. Clark, C. M. Huntington, C. C. Kuranz, A. R. Miles, S. R. Nagel, K. S. Raman, and V. A. Smalyuk, **116**, 18233 (2019).
[17]Y. Zhou, T. T. Clark, D. S. Clark, S. Gail Glendinning, M. Aaron Skinner, C. M. Huntington, O. A. Hurricane, A. M. Dimits, and B. A. Remington, Physics of Plasmas **26**, 080901 (2019).
[18]D. C. Eder, A. E. Koniges, O. L. Landen, N. D. Masters, A. C. Fisher, O. S. Jones, T. I. Suratwala, and L. J. Suter, Journal of Physics: Conference Series **112**, 032023 (2008).
[19]B. J. Le Galloudec, P. A. Arnold, E. G. Carroll, G. F. James, T. S. Runtal, D. M. Acosta-Lech, T. L. Bettis, J. D. Foley, A. Harkey, C. M. Jones, N. Lao, M. E. Mcintosh, M. A. Munguia, H. V. Nghiem, D. A. Schwedler, and D. R. Taylor, in *2017 IEEE 21st International Conference on Pulsed Power (PPC)* (2017), pp. 1–4.
[20]J. D. Moody, A. Johnson, J. Javedani, E. Carroll, J. Fry, B. Kozioziemski, S. O. Kucheyev, B. G. Logan, B. B. Pollock, H. Sio, D. Strozzi, W. A. Stygar, V. Tang, and S. Winters, Physics of Plasmas **27**, 112711 (2020).
[21]S. Chandrasekhar, *Hydrodynamic and Hydromagnetic Stability* (Oxford Univ. Press, Oxford, England, 1961).
[22]R. S. Cohen, L. Spitzer, and P. M. Routly, Phys. Rev. **80**, 230 (1950).
[23]J. Jukes, Journal of Fluids Mechanics **16**, 177 (1963).
[24]D. Batani, J. R. Davies, A. Bernardinello, F. Pisani, M. Koenig, T. A. Hall, S. Ellwi, P. Norreys, S. Rose, A. Djaoui, and D. Neely, Phys. Rev. E **61**, 5725 (2000).
[25]T. R. Mattsson and M. P. Desjarlais, Phys. Rev. Lett. **97**, 017801 (2006).
[26]M. J.-E. Manuel, A. B. Sefkow, C. C. Kuranz, A. M. Rasmus, S. R. Klein, M. J. MacDonald, M. R. Trantham, J. R. Fein, P. X. Belancourt, R. P. Young, P. A. Keiter, B. B. Pollock, J. Park, A. U. Hazi, G. J. Williams, H. Chen, and R. P. Drake, Phys. Rev. Lett. **122**, 225001 (2019).
[27]R. M. Darlington, T. L. McAbee, and G. Rodrigue, Comp. Phys. Comm. **135**, 58 (2001).
[28]C. M. Huntington, A. Shimony, M. Trantham, C. C. Kuranz, D. Shvarts, C. A. Di Stefano, F. W. Doss, R. P. Drake, K. A. Flippo, D. H. Kalantar, S. R. Klein, J. L. Kline, S. A. MacLaren, G. Malamud, A. R. Miles, S. T. Prisbrey, K. S. Raman, B. A. Remington, H. F. Robey, W. C. Wan, and H.-S. Park, Physics of Plasmas **25**, 052118 (2018).
[29]B. K. Shivamoggi, Physica Scripta **24**, 49 (1981).
[30]For this study, we do not vary the chemical composition of the CHI from its normal value, $C_{50}H_{47}I_3$, only the density.
[31]S. W. Haan, Phys. Rev. A **39**, 5812 (1989).
[32]A. Do, L. A. Pickworth, B. J. Kozioziemski, A. M. Angulo, G. N. Hall, S. R. Nagel, D. K. Bradley, T. Mccarville, and J. M. Ayers, Appl. Opt. **59**, 10777 (2020).
[33]J. A. Koch, O. L. Landen, B. J. Kozioziemski, N. Izumi, E. L. Dewald, J. D. Salmonson, and B. A. Hammel, Journal of Applied Physics **105**, 113112 (2009).
[34]J. Edwards, S. G. Glendinning, L. J. Suter, B. A. Remington, O. Landen, R. E. Turner, T. J. Shepard, B. Lasinski, K. Budil, H. Robey, J. Kane, H. Louis, R. Wallace, P. Graham, M. Dunne, and B. R. Thomas, Physics of Plasmas **7**, 2099 (2000).
[35]D. Strozzi, J. Moody, B. Pollock, H. Sio, G. Zimmerman, D. Ho, S. Kucheyev, C. Walsh, and B. Logan, Bulletin of the American Physical Society (2021).
[36]E. Epperlein and M. Haines, The Physics of fluids **29**, 1029 (1986).